Directing the mechanism of CO_2 reduction by a Mn catalyst through surface immobilisation.

James J. Walsh[a,b*], Mark Forster[c], Charlotte L. Smith[c], Gaia Neri[c], Richard J. Potter[d] and Alexander J. Cowan[c]

a: School of Chemical Sciences, Dublin City University, Glasnevin, Dublin 9, Ireland.

b: National Centre for Sensor Research, Dublin City University, Glasnevin, Dublin 9, Ireland.

c: Stephenson Institute for Renewable Energy, University of Liverpool, L69 7ZF, UK.

d: School of Engineering, George Holt Building, Brownlow Hill, University of Liverpool, L69 3GH, UK.

* To whom correspondence should be addressed. Email: james.walsh@dcu.ie

Electronic Supplementary Information

Contents

1 Experimental

1.1 Materials – Complex **3**, [Mn(bpy)$(COOH)_2$]$(CO)_3$Br], was synthesised as described previously.[S1] Anatase nc-TiO_2 films were prepared by depositing commercial TiO_2 colloidal precursor (Dyesol 90-T) paste onto fluorine-doped tin oxide (FTO, TEC-15, Pilkington) or FTO coated with 20 nm of conformal TiO_2 by ALD. The slides were sonicated in ethanol for 20 minutes before deposition. The paste was deposited on the films and spread with a glass rod. The thickness was controlled by using scotch tape and was measured *via* profilometry to be approximately 8 µm. The films were heated to dryness at 100°C, followed by annealing in air at 450°C for 30 minutes. The slides were cut so that the geometric surface area of the nc-TiO_2 films was approximately 1 cm^2. Acetonitrile (spectroscopic grade, VWR) was not dried before use, as a trace quantity of protons from atmospheric water was desirable to

promote catalysis. Ferrocene (Fc, Sigma-Aldrich) was purified by sublimation before use. TiO_2 nanopowder (anatase, < 50 nm, Sigma-Aldrich), ethanol (VWR) and tetrabutylammonium hexafluorophosphate ($(But)_4N\ PF_6$, Sigma-Aldrich) were used as received. Argon (N6) and CO_2 (CP grade) were purchased from BOC.

1.2 Spectroscopic and electrochemical methods - All electrochemistry was performed using a PalmSens[3] potentiostat. Reference electrodes used were either a Ag wire pseudo-reference calibrated versus the Fc/Fc^+ couple, or a non-aqueous reference electrode, $Ag/AgNO_3$ (10 mM $AgNO_3$, 0.1 M $(But)_4N\ PF_6$, CH_3CN).

Gas chromatography was performed using an Agilent 6890N employing N6 helium as the carrier gas (5 $ml.min^{-1}$). A 5 Å molecular sieve column (ValcoPLOT, 30 m length, 0.53 mm ID) and a pulsed discharge detector (D-3-I-HP, Valco Vici) were employed. CO peak areas were quantified with multiple calibrant gas injections and were re-calibrated daily. Film thickness measurements were performed using an Ambios Technology XP200 profilometer.

FTIR spectroscopy of **3** on TiO_2 nanopowder was performed using a Bruker Vertex spectrometer operating in 'Easydiff' difference mode using blank TiO_2 as a reference, to analyse the binding modes of carboxylate groups on the surface. Adsorption was performed by stirring nanopowder TiO_2 in a *ca*. mM soaking solution of **3** in ethanol for 2 hours in the dark. The solid was then centrifuged off and washed thoroughly with ethanol before drying.

UV/Vis/NIR absorption data were obtained using a Shimadzu 2550 UV/Vis/NIR spectrophotometer in transmittance mode using either a 1 cm pathlength quartz cuvette, or by direct transmittance measurement through a film. For UV/Vis/NIR measurements of nc-TiO_2 and **3**/nc-TiO_2 a non-aqueous reference electrode, $Ag/AgNO_3$ (10 mM $AgNO_3$, 0.1 M $(But)_4N\ PF_6$, CH_3CN) and a Pt mesh counter electrode were used in 0.1 M $(But)_4N\ PF_6$, CH_3CN electrolyte. For the DCVA experiments an absorbance-time plot was recorded simultaneously with a cyclic voltammogram. The absorbance-time data were synchronised with the CV data and the time axis converted to the equivalent potentials. The dAbs/dt (ordinate) data are shown inverted, as described in ref 21.

For ATR-FTIR-SEC experiments, an FTO slide was cut to approximately 1 x 2 cm and sonicated in ethanol for 20 minutes to remove grease. Holes of approximatly 1 mm diameter were drilled either side of the centre of the slide using diamond-tipped drill bits and a Dremel drill, using a water bath to dissipate heat. The drilled slide was rinsed, sonicated, and fired in air 450°C for 30 minutes to ensure the surface was clean. When cooled, TiO_2 sol-gel was applied between the two drill holes as described in section 1.1 and shown in Scheme 1 (main text), annealed, and soaked with **3**. The **3**/nc-TiO_2 film was partially removed before analysis to reduce the surface area, leaving a **3**/nc-TiO_2 film of approximately 1 x 1 mm. Ag and Pt wires thin eneough to fit through the drill holes were secured in position using silicone rubber (RS Electronics) and left to dry in the dark. A drop of electrolyte (CH_3CN, 0.1 M $(But)_4N\ PF_6$, *ca*. 1 mM Fc) was applied directly to the diamond ATR crystal and the nc-TiO_2 film placed face down onto the crystal. The weight of the sample spread the electrolyte into a thin layer. While care was taken to deoxygenate the electrolyte before use and keep the whole experiment in the dark, some light and oxygen exposure is inevitable. A strip of carbon paper was used to make a connection with the underside of the FTO working electrode, while a clamp was used to carefully control the clips attached to the Pt wire counter and Ag wire pseudo-reference. Intermittently the electrolyte evaporated and had to be replaced. Ferrocene was added as a sacrifical oxidant to prevent

electrolyte decomposition at the Pt counter electrode. Potential steps increments of 0.05 V were applied and held until the current reached a steady state and the spectrum recorded (average of 32 scans). Potentials were recorded vs the Ag/Ag^+ pseudo-reference electrode. Spectra were recorded at a resolution of 4 cm^{-1}. The data presented in Fig. 3 have been offset for clarity and an air background subtracted. The potentials at which the three spectra shown were - 0.80, - 0.85 and - 0.90 V vs Ag/Ag^+.

1.3 Atomic layer deposition - The FTO electrodes were coated with ~20 nm of highly conformal TiO_2 by ALD using an Oxford Instruments OpAL reactor at 225°C. The reactor was modified by the addition of a process controlled 'hold' valve between the pump and the process chamber, enabling precursor 'soak' steps. Soak steps were used to increase the residence time of the Ti-precursor to ensure good film coverage and to improve film density. Prior to ALD of the TiO_2, the samples were exposed to three ALD cycles using trimethyl aluminium (TMA, supplied by SAFC Hitech) followed by distilled water (H_2O) using the following sequence:

{(30 ms TMA Dose)(10 s purge)(30 ms H_2O)(10 s purge)}

This TMA based treatment improves the nucleation and growth of the subsequent TiO_2 layer due to the so-called 'self-cleaning' effect [REF] of TMA.[S2] The TMA sequence is expected to introduce negligible Al_2O_3 onto the FTO surface. For the TiO_2 growth, titanium(IV) isopropoxide (≥97%, supplied by Sigma Aldrich) was used as a metal source and was introduced into the reactor via a high speed Swagelok ALD™ valve. The Ti-precursor was heated to 70°C and was transported to the reactor by vapour-draw with the 'hold' valve closed. The TiO_2 ALD cycle was defined by the following sequence:

{(1 s Ti-isopropoxide dose and hold)(10 s purge)(30 ms H_2O dose)(10 s purge)}

The number of ALD cycles required to give ~20 nm of TiO_2 was found to be 333 based on spectroscopic ellipsometry of Si(100) witness samples (virgin test grade, supplied by Compart Technologies Ltd) using a MM-16 Horiba JY ellipsometer.

2 Soaking of 3 onto nc-TiO_2 sol gel derived films

Ethanolic solutions of **3** were made up to *ca*. mM concentration (3 ml). As **3** is photounstable under ambient light exposure, the soaking solution was kept in the dark and covered in aluminium foil to prevent decomposition. After soaking for 2 hours or overnight the samples were removed and rinsed thoroughly with ethanol to remove any physisorbed material. The electrodes were then dried under a stream of compressed air and further dried under vacuum in a Schlenk tube covered carefully with aluminium foil for a further two hours. We found that if the films were not dried properly under vacuum the Mn complex had a tendency to desorb quickly upon redox cycling. The dried nc-TiO_2 electrodes appeared bright orange.

It is worth reiterating here the instability of **3**/nc-TiO_2 under ambient light conditions. A bright orange film left on the bench turns colourless in approximately one hour, so all experiments were carefully covered in aluminium foil.

The surface coverage, Γ, of **3** on nc-TiO_2 was calculated from the absorbance drop of the Mn MLCT transition at *ca*. 420 nm before and after soaking. We calculated the extinction coefficient of **3** in CH_3CN as 2360 $M^{-1}.cm^{-1}$ at 420 nm and used this value to calculate Γ.

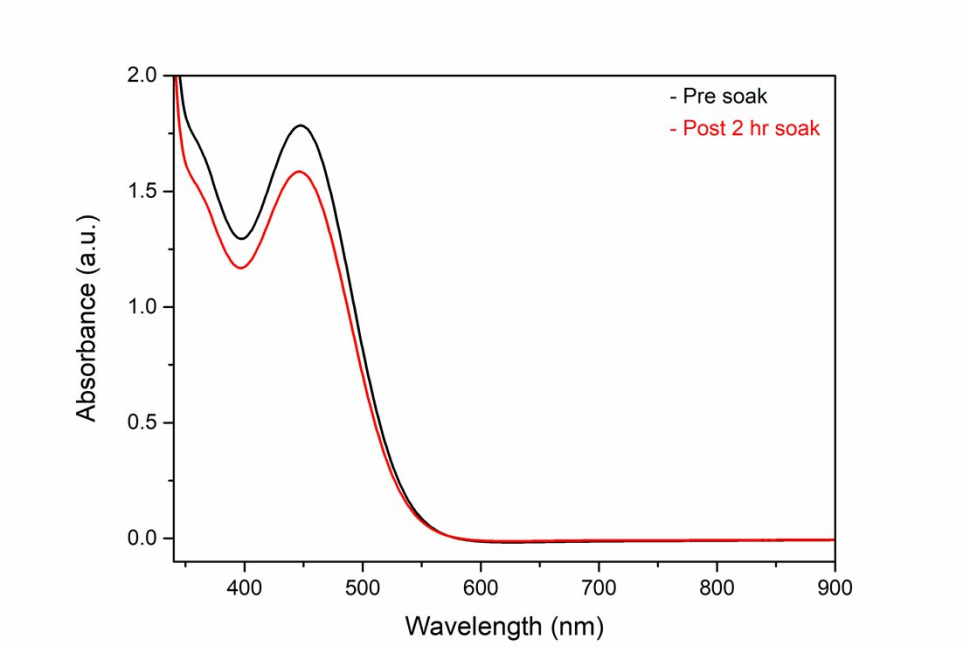

*Fig. S1: UV/Vis spectra of a solution of **3** before (black) and after 2 hr exposure to a nc-TiO_2 film (red).*

3 Voltammetry and scan rate dependence

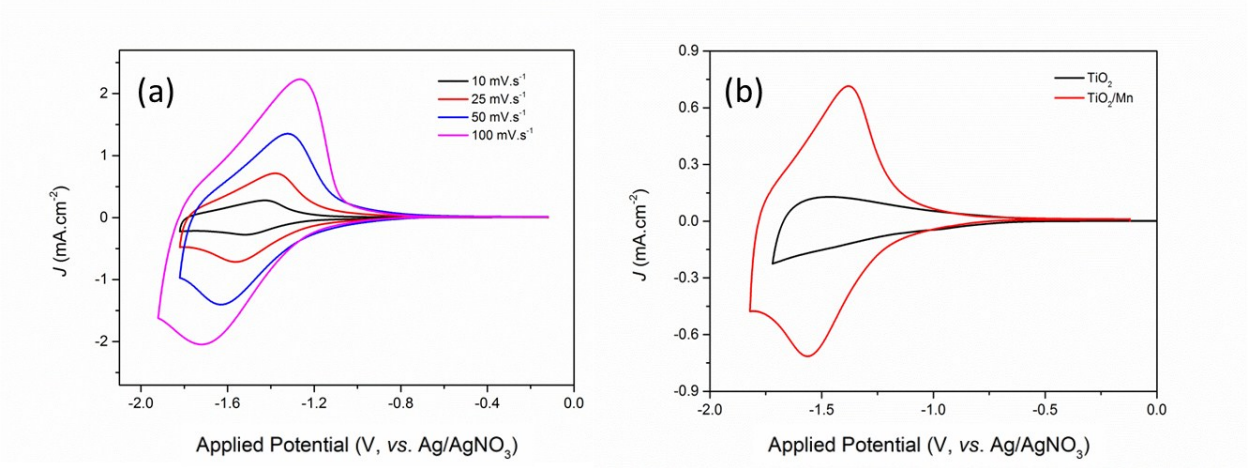

*Fig. S2 (a): Scan rate dependence of **3**/nc-TiO_2 in argon-purged CH_3CN/0.1 M $(But)_4N$ PF_6 at 100, 50, 25 and 10 mV.s^{-1}. Counter electrode: Pt basket, reference electrode: Ag/$AgNO_3$. (b) Comparison of **3**/nc-TiO_2 (red) and unmodified nc-TiO_2 (black) at 25 mV.s^{-1} under identical conditions.*

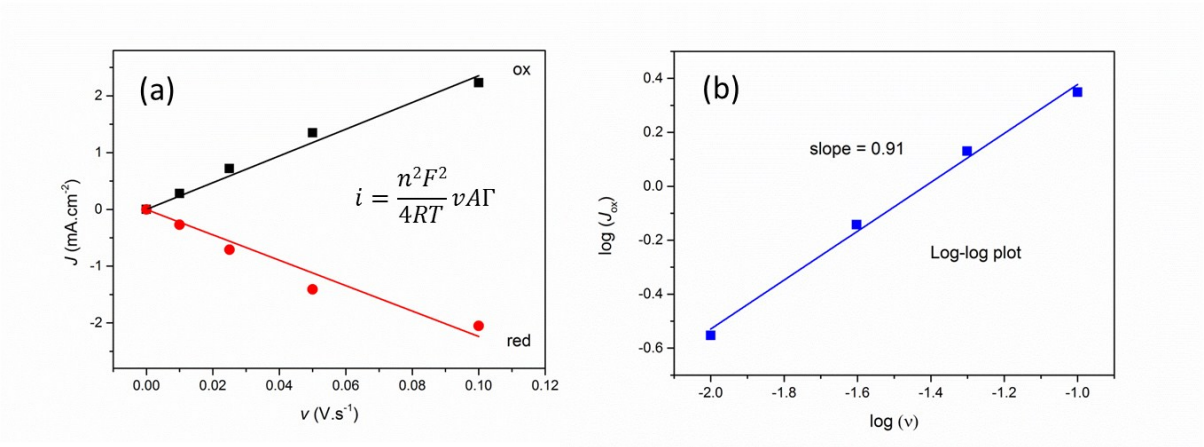

Fig. S3 (a): Linear plot of scan rate versus peak current density for the data in Fig. S2 (a). (b) log-log plot of scan rate vs. peak current density shows slope approaching 1.

Fig. S2 (b) shows clearly the presence of electroactive **3** on nc-TiO_2, while Fig. S3 (a) shows the species does not desorb irreversibly into the bulk. The slope approaching 1 in Fig. S3 (b) strongly suggests that **3**/nc-TiO_2 exhibits true surface confined voltammetry; in contrast a slope of 0.5 would suggest diffusion control according to the Randles-Sevçik equation. Collectively Figs. S2 and S3 also demonstrate stability towards redox cycling, as irreversible desorption would result in non-linear plots.

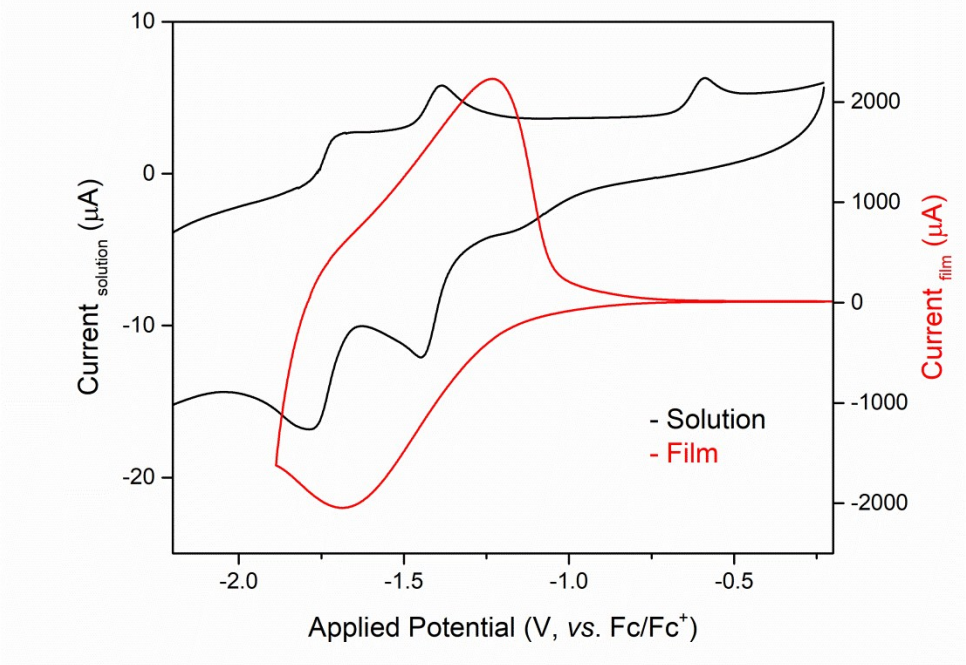

*Fig. S4 (a): CVs of **3** in CH_3CN/H2O (95:5)/0.1 M $(But)_4N$ PF_6 solution (black) and a film of **3**/nc-TiO_2 in CH_3CN/0.1 M $(But)_4N$ PF_6 (red). Both CVs were recorded at 100 mV.s^{-1} and corrected to a common reference scale (the Fc/Fc$^+$ couple).*

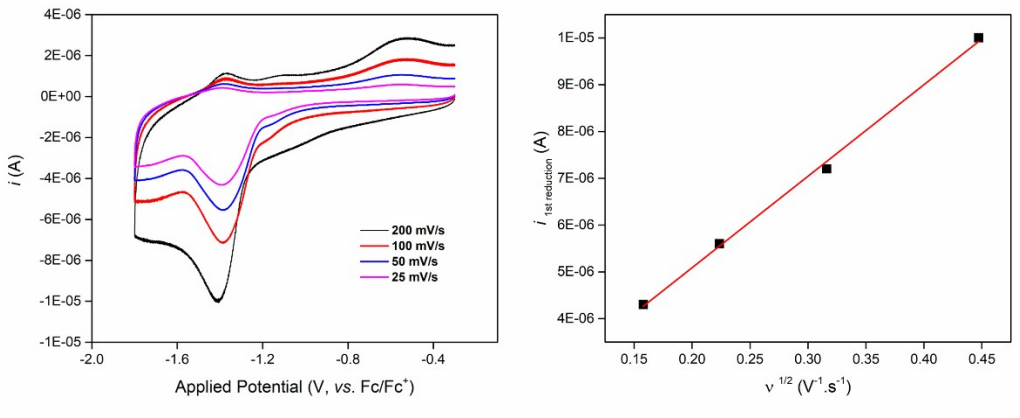

*Fig. S4 (b): CVs of **3** in CH_3CN/H_2O (95:5)/0.1 M $(But)_4N\ BF_4$ solution (left), and $v^{1/2}$ scan rate dependence on the current of the first reduction, indicating diffusion controlled redox behaviour. WE = glassy carbon, RE = $Ag/AgNO_3$ (corrected using Fc/Fc^+ couple) and CE = Pt wire.*

Fig. S4 (a) shows the differences in redox behaviour upon immobilisation of **3** on nc-TiO_2, relative to **3** in solution. The shifting of the two reduction potentials closer together is clearly observed. Fig. S4 (b) shows the scan rate dependence of **3** in *CH_3CN/H_2O (95:5)/0.1 M $(But)_4N\ BF_4$.*

4 UV/Vis/NIR spectroelectrochemistry (SEC)

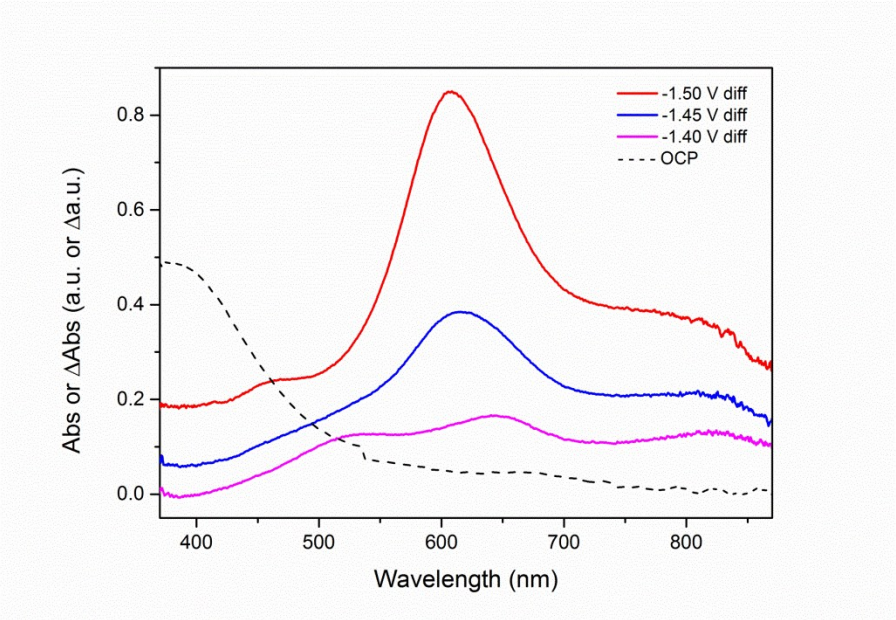

*Fig. S5: UV/Vis/NIR SEC of **3**/nc-TiO_2 at open circuit potential and at various potentials vs. $Ag/AgNO_3$.*

The stepwise formation of two new species is observed upon reduction. These two states can be related directly to Figs. 2 (a) and 3 in the main text, and correspond to the formation of dimeric **3** and doubly reduced **3**, respectively. Figs. 2, 3 and S5 demonstrate the power of spectroelectrochemical techniques over either CV or spectroscopy alone.

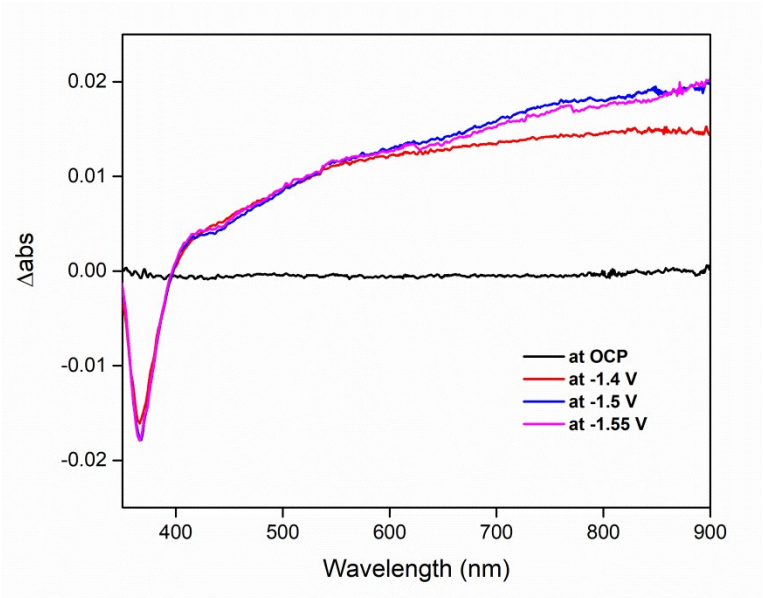

Fig. S6: UV/Vis/NIR SEC of nc-TiO_2 at open circuit potential and at various potentials vs. Ag/$AgNO_3$.

The stepwise reduction of unmodified nc-TiO_2 shows the grow-in of a vis/NIR absorption feature previously assigned to electrons trapped in the nc-TiO_2 conduction band.[S3] Spectrum at OCP was subtracted vs. itself.

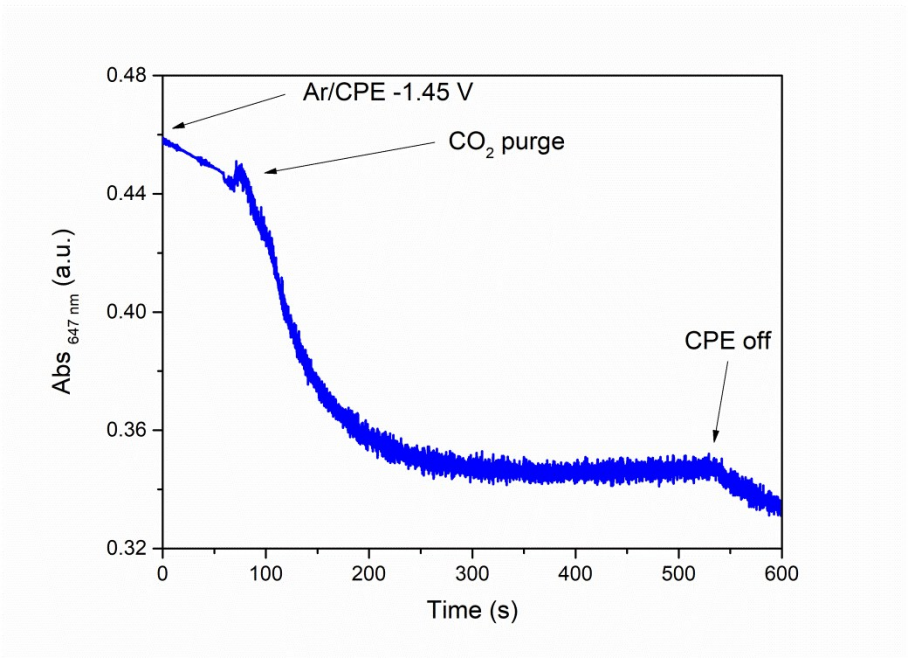

*Fig. S7: **3**/nc-TiO_2 film in argon-purged CH_3CN/0.1 M $(But)_4N$ PF_6, poised at -1.45 V vs. Ag/$AgNO_3$ to generate the adsorbed dimeric species. Upon CO_2-purging, the dimer absorption disappears.*

Upon reaction of dimeric **3** with CO_2 the absorption decrease unambiguously demonstrates catalysis mediated by dimeric **3**, corroborating our gas chromatographic data. This experiment is very similar

to the solution phase experiment of Bourrez *et al*. in the first report of dimer-mediated catalysis using $[Mn_2(dmbpy)_2(CO)_6]$ (where dmbpy = 4,4'-dimethyl-2,2'-bipyridine). See ref [S4].

5 FTIR of surface binding

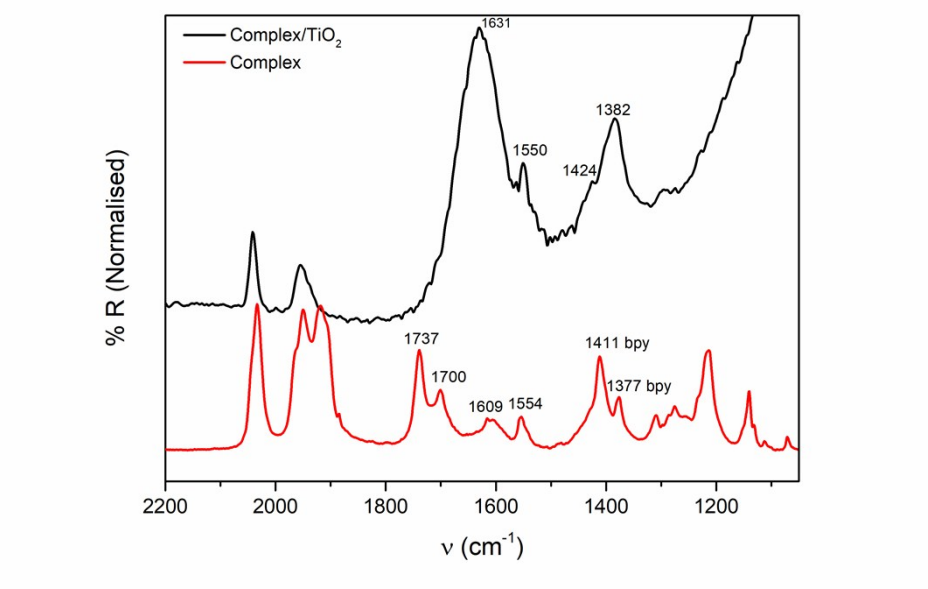

*Fig. S8: FTIR spectra of **3** and solid **3**/TiO_2.*

The FTIR spectra of TiO_2 surface bound carboxylates is a well-studied field, particularly with respect to dye-sensitised solar cells. The spectrum of solid **3** (red trace) shows the presence of three metal carbonyl stretches between 2100-1900 cm^{-1}, as well as symmetric carboxylic acid CO stretches at 1700 and 1738 cm^{-1}. Asymmetric and symmetric $\nu_{as}(CO_2^-)$ and $\nu_s(CO_2^-)$ stretches are visible at 1615 and 1308 cm^{-1} (giving a peak separation, $\nu_{as\text{-}s}$, of 307 cm^{-1}. In contrast, **3**/nc-TiO_2 shows no symmetric CO stretch around 1700 cm^{-1}, strongly implying that **3** on the surface of TiO_2 is only present in carboxylate form. $\nu_{as}(CO_2^-)$ and $\nu_s(CO_2^-)$ stretches are visible at 1628 and 1382 cm^{-1}, yielding a peak separation of 246 cm^{-1}. Previously, an empirical rule was published stating that band separation follows $\nu_{as\text{-}s}$ (monodentate) > $\nu_{as\text{-}s}$ (isolated) > $\nu_{as\text{-}s}$ (bidentate).[S5] The band splitting for **3** on nc-TiO_2 is larger than that of the free complex, implying bidentate surface co-ordination.

6 ATR-FTIR SEC data table

Species	Band positions (cm^{-1})	Reference
$[Mn(bpy(^tBu)_2)(CO)_3Br]$	2028 (s), 1933 (s), 1923 (s)	S5
$[Mn_2(bpy(^tBu)_2)_2(CO)_6]$	2025 (w), 1973 (s), 1928 (s), 1878 (m), 1850 (m), 1810 (w)	S5
$[Mn(bpy(^tBu)_2)(CO)_3]^-$ [b]	1973 (w), 1907 (s), 1807 (s)	S5
$[Mn(bpy(COO)_2)(CO)_3Br]$	2048 (s)[a], 2030 (s), 1947 (br)[a], 1932 (br)[a]	This work
$[Mn_2(bpy(COO)_2)_2(CO)_6]$	2025 (w), 1970 (s), 1927 (s), 1875 (m), 1847 (m), 1808 (w)	This work
$[Mn(bpy(COO)_2)(CO)_3]^-$ [b, c]	1970 (w), 1905 (s), 1805 (s)	This work

*Table S1: Metal carbonyl bands measured upon electrochemical reduction of **3** immobilised on nc-TiO_2 in CH_3CN/0.1 M $(But)_4N\ PF_6$ as shown in Fig. 3 (main text) and a direct comparison with (homogeneous) **2** in CH_3CN 0.1 M $(But)_4N\ PF_6$ solution. a: bands corresponding to the analogous solvated complex $[Mn(bpy(COO)_2)(CO)_3(CH_3CN)]^-$ formed spontaneously upon solvolysis in CH_3CN. See [S1] for further examples. b: The charge on this 5 co-ordinate complex is formally -1 in the case of $[Mn(bpy(^tBu)_2)(CO)_3]^-$; however in the case of $[Mn(bpy(COO)_2)(CO)_3]^-$ the formal charge is unclear as the protonation state of the four ligand-based carboxylic acid groups is not known in CH_3CN. The absence of symmetric v(CO) stretches at 1700-1740 cm^{-1} (as shown in Fig. S7) in the case of the adsorbed 5 co-ordinate complex imply that the complex is fully deprotonated; however the spectra are somewhat noisy in this region and definitive analysis of the carboxylate binding modes is not possible in this case. For the purposes of this discussion we use the -1 charge throughout this work. c: Some peaks from a residual dimer population are also observed between approximately 1930 and 2030 cm^{-1}. Legend: s = strong intensity, m = medium intensity, w = weak intensity, br = broad.*

The characteristic carbonyl stretching modes of the monomer complex are typical of a C_{3v} facial tricarbonyl complex (reported previously for Re analogues as one A1 mode at higher frequency and two E modes at lower frequency).[S6] The dimer spectrum consists of six modes, two of which are very weak, and by comparison with the number and position of metal carbonyl stretches reported for the dimer of complex **2** previously,[S7] a species with equivalent symmetry elements were inferred for **3** on nc-TiO_2. These assignments are also in-line with the related system $[Mn(bpy(PO_3H_2)_2)(CO)_3Br]$/nc-$TiO_2$.[S8] Finally, for the five co-ordinate species the spectrum is dominated by two major modes separated by *ca*. 100 cm^{-1} in the case of both **2** in CH_3CN and **3**/TiO_2.

References

S1 J. J. Walsh, C. L. Smith, G. Neri, G. F. S. Whitehead, C. M. Robertson and A. J. Cowan, *Faraday Discuss.*, 2015, **183**, 147–160.

S2 W. Jevasuwan, Y. Urabe, T. Maeda, N. Miyata, T. Yasuda, H. Yamada, M. Hata, N. Taoka, M. Takenaka and S. Takagi, *Materials*, 2012, **5**, 404–414.

S3 G. Neri, J. J. Walsh, C. Wilson, A. Reynal, J. Y. C. Lim, X. Li, A. J. P. White, N. J. Long, J. R. Durrant and A. J. Cowan, *Phys. Chem. Chem. Phys.*, 2015, **17**, 1562–1566.

S4 M. Bourrez, M. Orio, F. Molton, H. Vezin, C. Duboc, A. Deronzier and S. Chardon-Noblat, *Angew. Chem. Int. Ed.*, 2014, **53**, 240–243.

S5 C. Bauer, G. Boschloo, E. Mukhtar and A. Hagfeldt, *J. Phys. Chem. B*, 2002, **106**, 12693–12704.

S6 J. M. Smieja and C. P. Kubiak, *Inorg. Chem.*, 2010, **49**, 9283–9289.

S7 J. M. Smieja, M. D. Sampson, K. A. Grice, E. E. Benson, J. D. Froehlich and C. P. Kubiak, *Inorg. Chem.*, 2013, **52**, 2484–2491.

S8 T. E. Rosser, C. D. Windle and E. Reisner, *Angew. Chem. Int. Ed.*, 2016, **55**, 7388–7392.